Emission spectra of fullerenes: Computational evidence for blackbody-like radiation due to structural diversity and electronic similarity

Ozan Lacinbala [1,*] Florent Calvo [2] Cyril Falvo [1,2] Pascal Parneix [1]
Mathias Rapacioli [3] Aude Simon [3] and Thomas Pino [1,†]

[1]*Institut des Sciences Moléculaires d'Orsay, CNRS, Université Paris Saclay, 91405 Orsay, France*
[2]*LIPhy, CNRS, Université Grenoble Alpes, 38000 Grenoble, France*
[3]*Laboratoire de Chimie et Physique Quantiques, Fédération FeRMI, CNRS, 31062 Toulouse, France*

(Received 14 March 2023; revised 15 May 2023; accepted 19 May 2023; published 9 June 2023)

The spectral emission of hot C_{60} has been experimentally shown to be broad and continuous, in apparent contradiction with the discrete and narrow absorption spectrum associated with the high symmetry of buckminsterfullerene. In the present work we computationally model the emission spectrum of isolated carbon clusters, assuming a broad distribution of isomers that are likely populated under the experimental conditions. The contributions of individual structures to the global spectrum correspond to the relaxation via recurrent fluorescence and vibrational emission, electronic and vibrational structures being described by a simple but efficient density-functional-based tight-binding scheme. The model predicts a blackbody-like emission spectrum that is naturally broad and correctly accounts for the experimental measurements, except for a maximum that is quantitatively shifted with respect to Wien's displacement law. To quantify such differences, we introduce an emissivity parameter ε as the ratio between the spectral emittance and the corresponding exact blackbody spectrum; ε is numerically found to scale as $(\lambda T)^{-2}$ at leading order with increasing temperature T and for wavelengths $\lambda > 350$ nm, and we provide a theoretical justification for this behavior. Our results are discussed in the light of the astrophysical detection of interstellar fullerenes, as well as in combustion environments where carbon clusters are relevant in the context of nascent soot particle formation.

DOI: 10.1103/PhysRevA.107.062808

I. INTRODUCTION

The transition between bulklike continuous spectra and discrete molecularlike spectra in finite atomic systems has been a central issue in nanoscience for decades [1–3]. Thermal emission, which falls into this class, is well described in bulk materials based on quantum mechanical and statistical arguments, which notably lead to the Planck and Stefan-Boltzmann expressions for the blackbody spectrum and its integrated power, respectively.

The emission spectra of carbon clusters and fullerenes have received particular attention from various experimental groups, who reported blackbody-like emission spectra in the visible wavelength range for C_{60} [4,5] and smaller carbon clusters [6,7], arising from different heating processes that include laser desorption and laser-induced optical emission. More generally, the relaxation mechanisms of excited carbon clusters in the gas phase have been investigated in the past, with particular attention paid to thermionic emission in C_{60} [8–13], which was notably shown to also arise upon single-photon absorption [14]. Recently, radiative cooling was shown to be competitive with electron emission and fragmentation [15]. Models for radiative cooling based on the Stefan-Boltzmann equation have been developed to account for the observed dissociation behavior [16–18].

From these earlier efforts, it was clearly shown that radiative emission in carbon clusters in the gas phase mainly stems from electronic deexcitations rather than from the vibrational modes [16,19], with some notable exceptions such as the C_5^- [20] and C_7^- [21] anionic clusters. The featureless thermal emission spectra observed in hot fullerenes also contrast with the much better resolved electronic absorption spectrum measured for C_{60} at around 1000 K by Kataura *et al.* [22].

Several models were designed to explain the radiative cooling mechanisms in C_{60}, taking into account both the time-dependent relaxation processes and the spectral aspects of emitted photons [23–25], the optical response of buckminsterfullerene being typically treated based on a classical dielectric framework. While the timescales for radiative cooling inferred from these models generally agree with experimental measurements, the predicted emission spectra remain well resolved and differ sensitively from the broad blackbody-like profile, as a result of the discrete nature of the absorption cross section inherent to the dielectric model at low energies.

Two possible arguments were invoked to explain the continuous emission spectrum of buckminsterfullerene despite having highly discrete absorption bands, both involving the vibrational degrees of freedom either through the increasing interactions between electronic and vibrational excitations that enable forbidden transitions or through vibrational hot

*Present address: Quantum Solid-State Physics, Department of Physics and Astronomy, KU Leuven, Celestijnenlaan 200D, Leuven 3001, Belgium; ozan.lacinbala@kuleuven.be
†thomas.pino@universite-paris-saclay.fr

bands that cause line broadening [23,25,26]. Hansen *et al.* [27] used tight-binding linear-response theory to estimate the coupling between plasmons and normal vibrational modes in C_{60} buckminsterfullerene and found some slight smoothing in the absorption spectrum with increasing temperature. However, this work focused on rather high energies (5–30 eV) compared to the range relevant for thermal emission (less than 5 eV).

Earlier attempts at explaining the emission spectrum of C_{60} have assumed that the system resides solely in its most stable geometry as buckminsterfullerene. However, as is often the case in finite systems, C_{60} can isomerize and melt at sufficiently high temperature. Simulations by Kim and Tománek [28] notably showed that C_{60} becomes floppy above about 2000 K and isomerizes into branched carbon chains through a so-called pretzel phase near 4000 K. Nonfullerene 60-atom carbon clusters have also been reported in ion mobility experiments for cationic [29,30] and anionic [31] species produced by laser vaporization. Indirect evidence for nonfullerene carbon clusters is also found in combustion science, where the nature of nascent species bridging molecular compounds and soot particles in flames has remained elusive [32] and for which the accepted mechanisms [33–35] involve graphenelike carbon clusters also known as flakes. In astrochemistry, the conclusive detection of C_{60}, C_{60}^{+}, and C_{70} fullerenes in several interstellar environments [36–39] also suggests the presence of graphene flakes as intermediates along the fullerene road [40–42]. However, in contrast with ideal fullerenes, defective or even disordered carbon nanostructures have seldom been investigated [43].

In the present work we argue that structural diversity, as the result of the high temperatures reached under the experimental conditions of thermal emission, can explain the experimentally observed blackbody-like radiation from hot C_{60} through the collective emission of a broad sample of isomers. This idea has been explored in our previous works [26,44] and independently by other authors [45]. The collective emission stems from recurrent fluorescence (RF) taking place in individual carbon clusters. Recurrent fluorescence, also known as Poincaré fluorescence [46], has been identified in small polycyclic aromatic hydrocarbons [47,48] as well as metallic [49] and carbon [50,51] clusters. Our computational analysis relies on a database of structures collected using appropriate sampling methods [52] and for which the vibrational [53] and electronic [54] excited states are also available. Besides the broad spectral features, our model also reveals that the maximum in the emission spectrum occurs at a frequency that deviates from Wien's displacement law. As an extension of the bulk concept of emissivity, we quantify such deviations by evaluating a temperature- and frequency-dependent ratio ε between the calculated emission spectrum relative to the Planck blackbody spectrum. Our model indicates that this emissivity ε scales with wavelength λ and temperature T as $(\lambda T)^{-2}$ for $\lambda > 350$ nm, at leading order in $1/\lambda T$, a result recovered using simple theoretical arguments.

The article is organized as follows. In Sec. II we describe the computational approach used to determine the emission spectra of carbon clusters from the knowledge of their geometric and electronic features and establish the various approximations underlying the calculations. The resulting emission spectra at finite temperature are then presented in Sec. III and rationalized using a simple analytical model. In Sec. IV we introduce the emissivity and discuss its value and dependence on both wavelength and temperature. Section V provides some possible connections between the present work and its implications in the fields of combustion science and astrochemistry. Section VI summarizes the article.

II. METHOD

We consider the emission spectrum of a statistical sample of carbon cluster isomers, individually but independently excited at a fixed internal energy corresponding to typical temperatures in the range of 1500–3500 K, or a few tens of eV for the present systems. The main emission process is electronic radiative deexcitation because at internal energies considered in this work, vibrational emission is negligible compared to recurrent fluorescence [26].

To compute the recurrent fluorescence rate constants from all electronic excited states of each conformer, we use the optical spectra determined in our previous work [54] and obtained using the self-consistent charge density-functional-based tight-binding model [55] in its time-dependent version [56]. The model used to calculate vibrational emission and recurrent fluorescence rate constants, referred to as the time-dependent density-functional-based tight–binding (TD-DFTB) model in the present article, has been explained in detail in our previous work [26]. Briefly, radiationless transitions such as internal conversion, inverse internal conversion, and intramolecular vibrational redistribution are so fast compared to radiative transitions that the internal energy is assumed to be statistically redistributed among all accessible vibronic states between two such successive emission transitions. This allows occupation probabilities of vibronic states to be calculated in a microcanonical framework.

For any specific isomer, the recurrent fluorescence rate constants $A_{\rm rec}(\nu_n, E)$ associated with the transition $n \to 0$ from electronic excited state n with energy $h\nu_n$ down to the electronic ground state when the molecule has an internal energy E can be estimated from the microcanonical probability $p(h\nu_n, E)$ to occupy the nth electronic state as

$$A_{\rm rec}(\nu_n, E) = A_n p(h\nu_n, E), \tag{1}$$

where A_n is the electronic fluorescence rate constant of the $n \to 0$ transition. Here stimulated emission is neglected because under the very low photon density relevant to the present work, carbon clusters can be considered as isolated. The microcanonical probability can be expressed from the vibrational density of states (VDOS) $\rho_{\rm vib}^{(n)}(E)$ on the nth electronic state, taking into account the different ways of distributing the excess energy into available electronic states:

$$A_{\rm rec}(\nu_n, E) = A_n \frac{\rho_{\rm vib}^{(n)}(E - h\nu_n)}{\sum_k \rho_{\rm vib}^{(k)}(E - h\nu_k)}. \tag{2}$$

In the following, we approximate that, due to the large size of the clusters, the vibrational densities of states are very similar among electronic states in such a way that $\rho_{\rm vib}^{(n)}(E) \simeq \rho_{\rm vib}^{(0)}(E) = \rho_{\rm vib}(E)$. The denominator of Eq. (2) is next

rewritten by summing over available electronic states as

$$\sum_k \rho_{\rm vib}(E - h\nu_k) \simeq \int_0^{E/h} \rho_{\rm elec}(h\nu)\rho_{\rm vib}(E - h\nu)hd\nu, \quad (3)$$

where we have denoted by $\rho_{\rm elec}$ the density of electronic states, with $\rho_{\rm elec}(h\nu)dh\nu$ the number of electronic states lying between $h\nu$ and $h\nu + hd\nu$. The electronic fluorescence rate constants A_n are obtained from the relation [57]

$$A_n = \frac{2\pi e^2 \nu_n^3}{m_e \varepsilon_0 c^3} \frac{f_n}{\nu_n}, \quad (4)$$

with e the elementary charge, m_e the electron mass, ε_0 the vacuum permittivity, c the velocity of light in vacuum, and f_n the electronic oscillator strength corresponding to $n \to 0$ electronic transitions. In practice, to evaluate Eq. (2), we compute the VDOS from the harmonic frequencies of each isomer in the electronic ground state using the Beyer-Swinehart counting algorithm [58].

The upper limit in the integral above is the internal energy E deposited in the isomer. Reasonable estimates for this quantity can be inferred from the earlier work by Kim and Tománek [28], who found that fullerenes remain stable (undissociated) up to temperatures in excess of 3400 K. Temperatures and internal energies can be connected to one another by considering the definition valid for microcanonical systems

$$\frac{1}{k_B T} = \frac{1}{\rho_{\rm vib}} \frac{\partial \rho_{\rm vib}}{\partial E}, \quad (5)$$

which for the present 60-atom system yields $E = 42$ eV at 3400 K. At the lower temperatures of 1350 and 2400 K, the corresponding maximum energies for C_{60} isomers are found to be 12.5 and 27.5 eV, respectively. For C_{42} clusters, which are expected to be not as stable as C_{60}, only temperatures of 1350 and 2400 K will be considered, which correspond to upper internal energies of 9 and 19 eV, respectively.

To account for a population of isomers relevant at such high internal energies, we combine the emission spectra obtained from individual isomers into a collective spectrum by simple unweighted summation. The isomers themselves are selected from databases collected in our earlier work [52], using atomistic simulations and systematic sampling of the potential energy surfaces for both C_{60} and C_{42}, based on the second generation reactive bond-order potential [59]. In this work, it was also shown consistently with the results of Kim and Tománek [28] that the structures of carbon clusters can be classified into four main families essentially depending on their aromatic content and overall shape: cages, which include fullerenes; flakes, which can be defined as mostly planar polycyclic aromatic compounds; pretzel-like structures, with a more open character and long carbon chains; and branched structures with terminating sp carbons (see Fig. 1).

Summing the individual spectra into an effective, collective emission spectrum amounts to neglecting the populations expected at thermal equilibrium. However, the processes we are modeling here are strongly out of equilibrium and, perhaps more importantly, the electronic properties of the various isomers are found to be rather uncorrelated to their binding energy (this feature can be indirectly seen in Fig. 7 in Appendix A). This weak dependence on the specific isomer further allows us to ignore the contribution of isomerization processes in kinetic competition with photon emission itself. In addition to isomerization, we neglect in our modeling other decay mechanisms such as thermionic emission as well as atomic and molecular dissociation, for which the rate constants are expected to be much lower than those involving electronic transitions [60].

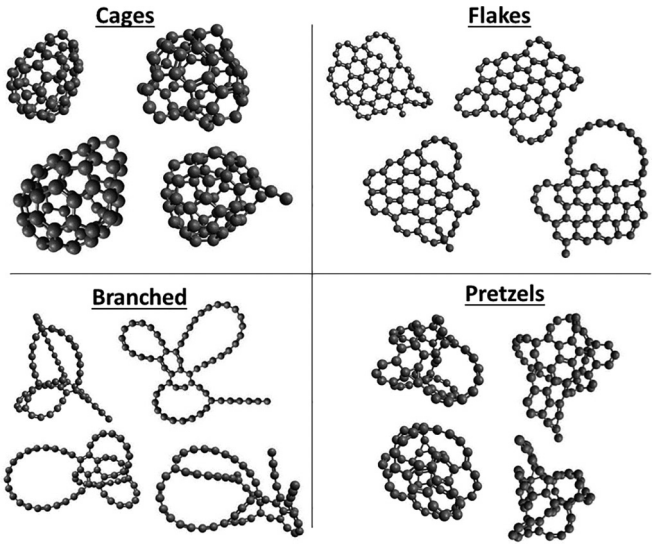

FIG. 1. Typical C_{60} structures from the four carbon cluster families considered in this work.

III. EMISSION SPECTRA: RESULTS FOR C_{60} AND C_{42}

Four emission spectra were determined from the different samples of isomers available for both C_{60} and C_{42} clusters, corresponding to the four families of cages, flakes, pretzels, and branched structures. Each sample contains 1000 structures and the raw spectra obtained from the numerical model were further convoluted with a Gaussian broadening function of 12.5 meV full width at half maximum. The combined effects of this parameter and the size of the sample are discussed in Appendix B.

The spectra were determined at different internal energies, corresponding for the various systems to different temperatures through Eq. (5). The effects of temperature, size, and structural family on the emission spectra are illustrated in Figs. 2–4, respectively. The results obtained in Fig. 2 for the cages sample of C_{60} at the temperatures of 1350, 2400, and 3400 K clearly illustrate the effects of structural diversity on the emission spectrum. These spectra exhibit a blackbody-like shape, which broadens and shifts to the blue as temperature increases. The specific contribution of vibrational bands (highlighted by vertical arrows in Fig. 2) is only seen at low energies compatible with the excitation of vibrational modes and tends to decrease relative to the contribution of electronic degrees of freedom at higher temperatures.

The spectra obtained at 1350 and 2400 K for C_{60} cages are shown again in Fig. 3, now in comparison to the spectra predicted for C_{42} cages. At the present numerical resolution and at fixed temperature, the normalized spectra are

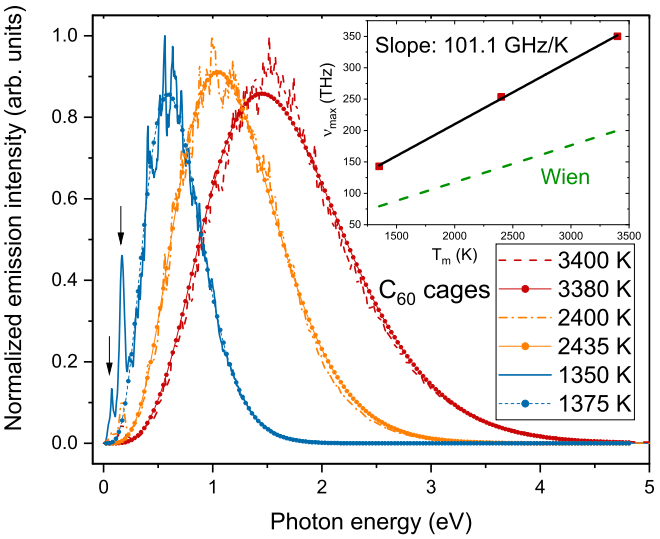

FIG. 2. Emission spectra obtained for C_{60} cage samples at three temperatures. The spectra have been convoluted by a Gaussian broadening function with a full width at half maximum of 12.5 meV and normalized at their respective maxima. The vertical arrows highlight the positions of the vibrational bands. The curves are the best fits using a modified Planck function $A\nu^5/(e^{\beta h\nu} - 1)$ in which the corresponding temperature is indicated. The inset shows the position of the maximum in the spectrum as a function of temperature (red squares). The black solid line is the corresponding linear fit, while the green dashed line shows the predictions from Wien's displacement law model.

essentially similar between the two samples, with common widths and positions of the maximum, the vibrational features at low energies also being common to the two samples. Moreover, as shown in Fig. 4 for the case of C_{60}, both the width and

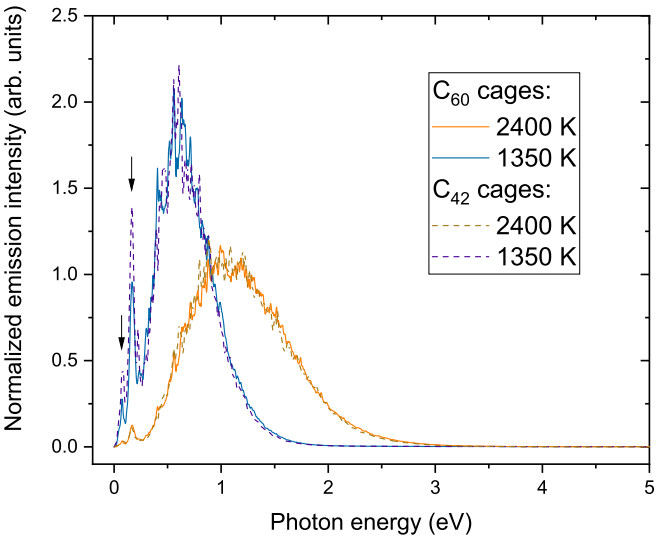

FIG. 3. Emission spectra obtained for C_{60} and C_{42} cage samples, at 1350 and 2400 K. The spectra have been convoluted by a Gaussian broadening function with a full width at half maximum of 12.5 meV and they are normalized by their respective integrals. The vertical arrows highlight the positions of vibrational bands.

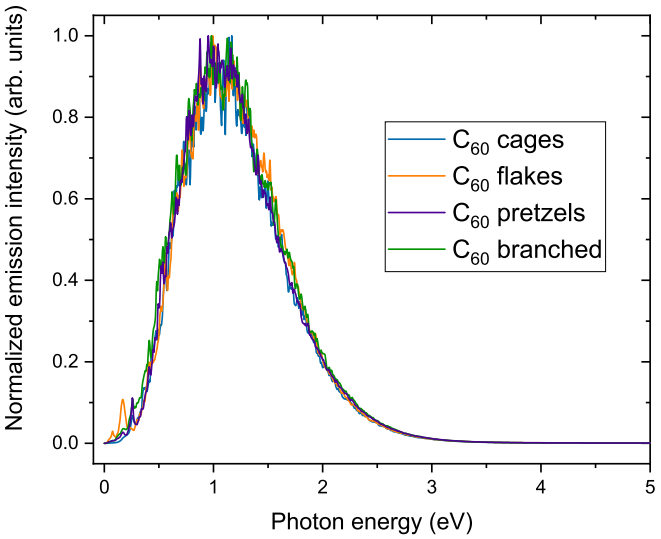

FIG. 4. Emission spectra obtained for C_{60} carbon clusters at 2400 K in their different structural families.

the maximum position display very minor dependences on the structural type. Our model thus shows that statistical considerations of the underlying structures that are responsible for the emitted radiation suffice to produce a broad continuous emission spectrum that depends on size and structural details only marginally, though more sensitively on temperature.

Wien's displacement law predicts that for a true blackbody spectrum the maximum position $\nu_{\max}$ scales with (canonical) temperature T such that $\nu_{\max}/T = 58.8\ \mathrm{GHz\,K^{-1}}$. From our numerical simulations, we find indeed that $\nu_{\max}$ scales linearly with T but with a different slope equal to $\nu_{\max}/T \simeq 101\ \mathrm{GHz\,K^{-1}}$, as shown in the inset of Fig. 2. Such a deviation from Wien's displacement law in our numerical results suggests that the original Planck function for blackbody radiation, from which the displacement law derives, cannot correctly account for the presently obtained emission spectra. We have attempted to adjust the numerical spectra using a generalized Planck function

$$B_p(\nu, T) \propto \frac{\nu^p}{\exp(h\nu/k_{\mathrm{B}}T) - 1}, \tag{6}$$

with p a parameter normally equal to 3 in the original Planck model. The best fit to the calculated spectra is obtained for $p \approx 5$, the resulting functions being superimposed on the data in Fig. 2. In the following section we attempt to rationalize this behavior using simple theoretical arguments.

IV. A SIMPLE MODEL FOR THE SPECTRAL EMITTANCE

The spectral emittance of carbon clusters can be estimated using reasonable approximations regarding the vibrational and electronic densities of states. We assume that the emitted photons mainly originate from recurrent fluorescence and proceed to evaluate the emittance M_{elec} expressed as the product between the RF rate constant A_{rec} and the density of electronic states over the sample ρ_{elec} as

$$M_{\mathrm{elec}}(\nu, E) = \frac{h\nu}{S} A_{\mathrm{rec}}(\nu, E)\rho_{\mathrm{elec}}(\nu), \tag{7}$$

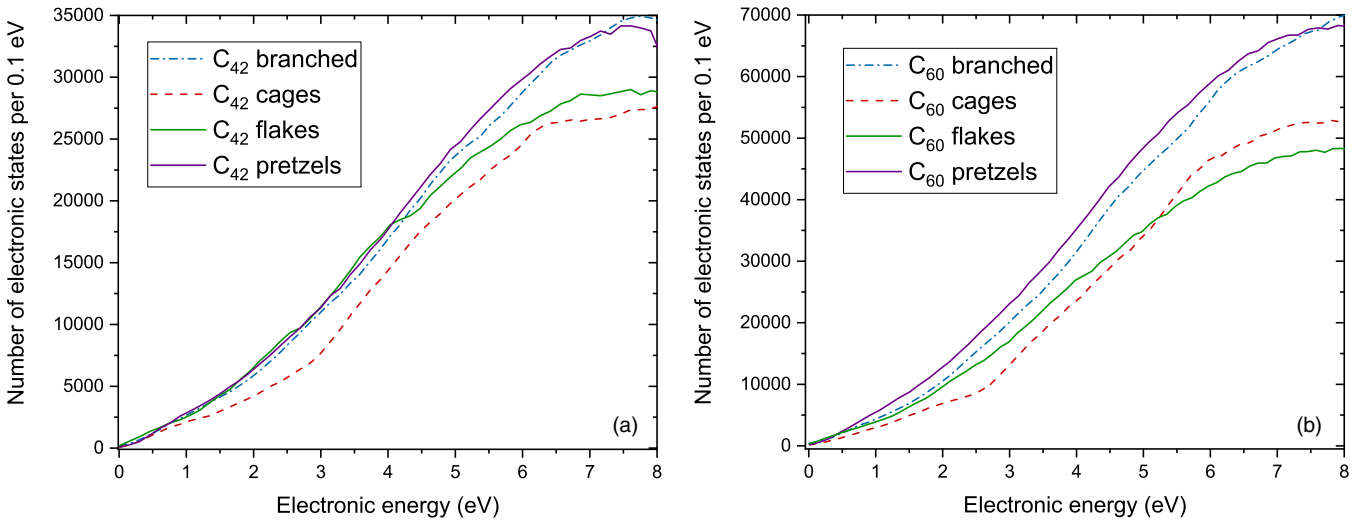

FIG. 5. Electronic densities of states obtained from TD-DFTB data for the four structural families of (a) C_{42} and (b) C_{60} cluster samples, accumulated over 1000 isomers in each sample and using a bin size of 0.1 eV.

with $S = 4\pi\langle R_g\rangle^2$ the mean exposed area and $\langle R_g\rangle$ the mean gyration radius.

To evaluate the RF rate constant, an explicit form is needed for the vibrational density of states and a natural choice is provided by performing a semiclassical approximation as [61]

$$\rho_{\rm vib}(E) \approx a(E + E_z)^{s-1}, \tag{8}$$

with E the vibrational energy, E_z the zero-point energy, $s = 3N - 6$ the number of vibrational degrees of freedom of the N-atom system, and a a positive constant. In the following, we further exploit that $s \gg 1$ for both C_{42} ($s = 120$) and C_{60} ($s = 174$), allowing us to assimilate $s - 1$ as s for simplifying purposes. For the present harmonic systems, the semiclassical approximation above is expected to be exact in the limit of high internal energies. It predicts a linear relation between internal energy and temperature as $E + E_z \simeq sk_BT$. Figure 9 in Appendix C compares this linear relation with Eq. (5) and shows that it is accurate for internal energies above approximately 20 eV for C_{60} and above approximately 15 eV for C_{42}.

The electronic contribution appearing in Eq. (3) can also be approximated with simple functions, here using a linear relation

$$\rho_{\rm elec}(\nu) \approx K h\nu, \tag{9}$$

with K a positive factor. Such a linear correspondence is numerically justified by considering the actual densities of electronic states obtained from the TD-DFTB data accumulated over the samples for both C_{42} and C_{60}, which are represented in Fig. 5. As shown in this figure, in the relevant range below 4 eV, the variations of $\rho_{\rm elec}$ with increasing energy show a weak dependence on the structural family and are always approximately linear. The numerical values of K found for the various samples of C_{42} and C_{60} are given in Table I. They fall in the range of 25–80 eV^{-2} and increase with the degree of disorder (the sp/sp^2 fraction) in the cluster.

Using Eqs. (8) and (9), the RF rate constant of Eq. (2) can be expressed as

$$A_{\rm rec}(\nu, E) = \frac{A(\nu)}{K} \frac{\left(1 - \frac{h\nu}{E+E_z}\right)^s}{\int_0^E h\nu\left(1 - \frac{h\nu}{E+E_z}\right)^s d(h\nu)}, \tag{10}$$

with $A(\nu)$ the electronic fluorescence rate constant from the electronic state with energy $h\nu$. The next step is to evaluate the integral in the denominator. In this purpose we account for that photon energies are much lower than the internal energy and we perform a Taylor expansion in $h\nu/(E + E_z)$, leading to

$$\left(1 - \frac{h\nu}{E + E_z}\right)^s \simeq \exp\left[-\frac{sh\nu}{E + E_z} + \frac{1}{2s}\left(\frac{sh\nu}{E + E_z}\right)^2\right]. \tag{11}$$

TABLE I. Linear rate of variation K of the electronic density of states, and average quantities $U = \langle f(\nu)/\nu\rangle$ and $\langle R_g\rangle$ over carbon cluster samples for the four families of C_{42} and C_{60}. Also included are the values obtained from Eqs. (16) and (25) for the prefactor $C(s)$ and the total emissivity $\varepsilon_{\rm tot}$ associated with each sample.

Parameter	Cages	Flakes	Pretzels	Branched
C_{60}				
K (eV^{-2})	40	60	71	81
U (10^3 eV^{-1})	1.5	4.7	2.4	10.1
$\langle R_g\rangle$ (Å)	3.60	5.16	4.21	6.39
$C(s)$ (10^{50} eV^3 $\mathrm{s}^3/\mathrm{Å}^2$)	4.9	7.4	5.7	10.4
$\varepsilon_{\rm tot} \times 10^4$	1.8	2.8	2.1	3.9
C_{42}				
K (eV^{-2})	25	42	40	39
U (10^3 eV^{-1})	1.8	3.9	2.4	9.0
$\langle R_g\rangle$ (Å)	3.04	4.28	3.63	5.29
$C(s)$ (10^{50} eV^3 $\mathrm{s}^3/\mathrm{Å}^2$)	8.2	9.0	7.6	13.5
$\varepsilon_{\rm tot} \times 10^4$	3.1	3.4	2.9	5.1

The integral in the denominator of Eq. (10) can thus be rewritten as

$$\int_0^E h\nu\left(1-\frac{h\nu}{E+E_z}\right)^s d(h\nu) = \left(\frac{E+E_z}{s}\right)^2 \int_0^{sE/(E+E_z)} xe^{-x}e^{-(1/2s)x^2}dx. \quad (12)$$

For the present systems, the upper integration limit $sE/(E+E_z)$ exceeds 100 for all temperatures and sizes, providing as our next approximation

$$\int_0^{sE/(E+E_z)} xe^{-x}e^{-(1/2s)x^2}dx \simeq \int_0^{\infty} xe^{-x}dx = 1 \quad (13)$$

and leading to a RF rate constant given by

$$A_{\mathrm{rec}}(\nu,E) = \frac{A(\nu)}{K}\left(\frac{s}{E+E_z}\right)^2\left(1-\frac{h\nu}{E+E_z}\right)^s. \quad (14)$$

The RF rate constant $A(\nu)$ also depends on the electronic excited states involved through at least the prefactor A_n of Eq. (4). It notably contains the ratio f_n/ν_n for transitions $n \to 0$, whose numerical examination reveals that this quantity does not depend strongly on either n or the specific isomer considered (see Fig. 7 in Appendix A). We thus assume a constant value for $U = \langle f(\nu)/\nu\rangle$, which we take as the average over the 300 lowest excited states from the sample.

From Eqs. (4), (9), and (14), and invoking the linear relation between internal energy and temperature arising from the semiclassical approximation for $\rho_{\mathrm{vib}}(E)$, the spectral emittance then reads

$$M_{\mathrm{elec}}(\nu,E) = C\frac{\nu^5}{(k_{\mathrm{B}}T)^2}\left(1-\frac{h\nu}{E+E_z}\right)^s. \quad (15)$$

The prefactor C depends on the details of the sample considered through the factor U and the mean gyration radius $\langle R_{\mathrm{g}}\rangle$ as

$$C(s) = \frac{e^2h^3}{2m_{\mathrm{e}}\varepsilon_0 c^3}\frac{U}{\langle R_{\mathrm{g}}\rangle^2} \quad (16)$$

and thus depends on the size s mainly through the radius of gyration $\langle R_{\mathrm{g}}\rangle$ and, more implicitly, on some structural details of the sample. The values of these quantities obtained for the various samples are given in Table I.

From Eq. (11), the emittance can be finally rewritten as

$$M_{\mathrm{elec}}(\nu,E) = C\beta^2\nu^5\exp\left(-\beta h\nu + \frac{1}{2s}(\beta h\nu)^2\right), \quad (17)$$

in which the ν^5 behavior is recovered and $\beta = 1/k_{\mathrm{B}}T$. This ν^5 dependence of the emittance is understood as follows: (i) A linear contribution comes from the spectral density of electronic states over the sample of isomers (Fig. 5); (ii) another linear contribution comes from the energy $h\nu$ of emitted photons (this contribution is also involved in the Planck function); and (iii) a cubic dependence stemming from spontaneous emission that itself decomposes into two contributions, one linear dependence from the electric dipole transition moment and a quadratic dependence from the spectral density of electromagnetic modes (also involved in the Planck function).

Another difference between the results presently obtained for finite system samples and the blackbody emittance is suggested by Eq. (17), which scales as $1/T^2$ at low frequencies $h\nu \ll k_{\mathrm{B}}T$. This behavior contrasts with the Rayleigh-Jeans law in which the emittance scales linearly with temperature and can be traced back to Eq. (3) expressing the sharing between electronic and vibrational energies in isolated systems. Due to this contribution, low-lying electronic states become depopulated in favor of higher states as temperature increases, a depopulation effect that does not occur for photon modes, which explains why the maximum in blackbody emission spectra increases with temperature.

In the light of this simple model, the similarity between the emission spectra obtained at the same temperature in Figs. 3 and 4 is explained by a combination of factors, namely, (i) the overall behavior of the density of electronic states as a function of energy is the same for all C_{60} and C_{42} families (see Fig. 5); (ii) the electronic states are mainly populated according to the internal energy of the isomers; and (iii) the electronic dipole transition moments are essentially uncorrelated to the electronic states of their family (see Fig. 7 in Appendix A). Thus, the influence of geometrical structure of the various families resides in the vibrational contribution of the emission spectra, which lies below 0.5 eV, and in the gyration radius $\langle R_g\rangle$, albeit to a much lesser extent.

The difference between the thermal emission of carbon clusters obtained in the present computational model and the predictions from the standard Planck model for blackbody radiation can be quantified by introducing a dimensionless emissivity ratio ε defined for any canonical temperature as [62]

$$\varepsilon(\nu,T) = \frac{M_{\mathrm{elec}}(\nu,T)}{M^{\circ}(\nu,T)}, \quad (18)$$

with M_{elec} the spectral emittance resulting from the sample of carbon clusters and expressed in Eq. (17). Here M° is the blackbody spectral emittance expressed by the well-known Planck function as

$$M^{\circ}(\nu,T) = \frac{2\pi h\nu^3}{c^2}\frac{1}{\exp\left(\frac{h\nu}{k_{\mathrm{B}}T}\right)-1}. \quad (19)$$

Invoking the Planck model to describe the results obtained here for systems under isolated conditions requires using the proper thermodynamical definition of temperature, which is provided by Eq. (5) or, in our semiclassical approximation, by the simple linear relation $E + E_z = sk_{\mathrm{B}}T$. The microcanonical and canonical relations between energy and temperature are known to agree well with one another except in the vicinity of phase transitions [63].

A total emissivity ratio $\varepsilon_{\mathrm{tot}}$ that only depends on temperature can likewise be defined by summing the corresponding emissivities on frequency as

$$\varepsilon_{\mathrm{tot}} = \frac{\int_0^{\infty} M_{\mathrm{elec}}(\nu,T)d\nu}{\int_0^{\infty} M^{\circ}(\nu,T)d\nu}. \quad (20)$$

The denominator is given by the Stefan-Boltzmann law and reads

$$\int_0^{\infty} M^{\circ}_{\mathrm{elec}}(\nu,T)d\nu = \sigma T^4, \quad (21)$$

with $\sigma = 2\pi^5 k_B^4/15h^3c^2$ the Stefan-Boltzmann constant.

In our model for finite systems, a temperature-dependent emissivity parameter $\varepsilon(\nu, T)$ can likewise be defined, using Eq. (17) for the numerator, keeping the Planck function of Eq. (19) as the denominator and using again the semiclassical relation $E + E_z = sk_BT$ to connect energies and temperatures to each other. It can be straightforwardly shown that $\varepsilon(\nu, T)$ depends on temperature and frequency only through the product $x = \beta h\nu$:

$$\varepsilon(\nu, T) = \frac{C(s)c^2}{2\pi h}\frac{\beta^2\nu^5}{\nu^3}\frac{\exp[-\beta h\nu - (\beta h\nu)^2/2s]}{\exp(\beta h\nu) - 1}$$
$$\approx \gamma(s)x^2\exp(-x^2/2s). \quad (22)$$

Here we have further approximated the denominator in the Planck function as $\exp(\beta h\nu)$, valid at leading order in $\exp(-\beta h\nu)$, and we introduced a constant factor γ that only depends on the sample and on size s through the quantity $C(s)$. This factor can be expressed as a simple function of ε_{tot}, and we proceed by evaluating this other quantity. Integrating Eq. (17) over frequencies, we obtain

$$\int_0^\infty M_{elec}(\nu, T)d\nu = C(s)\beta^2\int_0^\infty \nu^5 e^{-\beta h\nu-(1/2s)(\beta h\nu)^2}d\nu$$
$$= \frac{C(s)}{\beta^4h^6}\chi(s), \quad (23)$$

where we have introduced the integral $\chi(s)$ as

$$\chi(s) = \int_0^\infty x^5\exp\left(-x - \frac{x^2}{2s}\right)dx, \quad (24)$$

leading to our final expression for the total emissivity parameter as

$$\varepsilon_{tot}(s) = \frac{k_B^4}{\sigma h^6}\chi(s)C(s). \quad (25)$$

The values of ε_{tot} obtained for the various samples of structures are given in Table I, whereas $\chi(s) \simeq 102$ for C_{42} and $\chi(s) \simeq 107$ for C_{60}. Note that, unlike $C(s)$, which depends on the statistical details of the sample through the values of U and $\langle R_g\rangle$, χ only depends on cluster size N through $s = 3N - 6$.

Combining Eqs. (22) and (25), the emissivity parameter ε is thus found to depend on temperature and frequency through

$$\varepsilon(\nu, T) = \frac{\pi^4}{15\chi(s)}\varepsilon_{tot}(s)(\beta h\nu)^2e^{-(\beta h\nu)^2/2s} = \varepsilon(\beta h\nu). \quad (26)$$

This relation indicates that the emissivity should vary with $x = \beta h\nu$ as $\varepsilon(x) \propto x^2\exp(-x^2/2s)$. Figure 6, in which a reduced emissivity $\varepsilon(x)\exp(x^2/2s)$ is represented in double logarithmic scale against x, confirms the expected quadratic behavior.

For large enough $\beta h\nu$, the emissivity of carbon clusters due to recurrent fluorescence can thus be well described by our model and Eq. (26). Two physical ingredients were instrumental in establishing this relation, both involving the statistical properties of the electronic excited states: (i) the linear dependence of the electronic density of states with increasing energy; and (ii) the approximate lack of correlation between the electric dipole transition moment to the ground state from a specific excited state with the energy of this excited state. Another difference of the conventional Planck model for blackbody radiation lies in the extra $1/T^2$ scaling of the emissivity found in our model. This factor stems from the T^2 dependence in the number of accessible vibronic states and conveys a depletion in the population of low-lying electronic states as temperature increases.

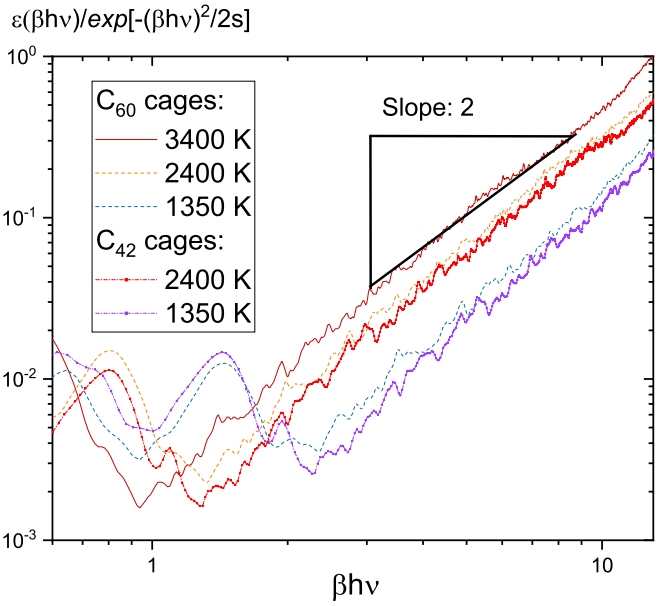

FIG. 6. Mean emissivities for the cage samples of C_{60} and C_{42} represented at different temperatures normalized by $\exp[-(\beta h\nu)^2/2s]$, shown as a function of the dimensionless quantity $\beta h\nu$. The quadratic behavior is emphasized in the regime $\beta h\nu > 2$.

Deviations to the generic behavior of Eq. (26) are found for $\beta h\nu < 2$, a range in which the approximations made in our derivation are no longer valid. In this regime, vibrational bands are stronger than the continuum emission due to recurrent fluorescence. From the viewpoint of excited electrons, the heat bath is provided by the available vibrational energy. At sufficiently high temperature or for low excited electronic states, $\beta h\nu$ is small and the Gaussian term in Eq. (26) becomes negligible, meaning that the heat bath is very large compared to the emitting electronic state. As $\beta h\nu$ decreases further, the canonical framework becomes more appropriate to describe the system and the Gaussian term in Eq. (26) appears as a second-order correction accounting for the finite size of the clusters.

According to our derivation, the emissivity $\varepsilon(\beta h\nu)$ obtained for the different samples and at various temperatures fall onto a single curve that only depends on s through the parameter $\chi(s)$ in Eq. (26). In practice, some residual vertical shifts are found for both cluster sizes, indicating a minor but additional temperature dependence of the prefactor ε_{tot} that is ignored by our model. Such a discrepancy can be traced back to the semiclassical approximation of Eq. (8), which is found to be inadequate at energies below 10–15 eV depending on system size. This is illustrated in Fig. 9 in Appendix C, where the VDOSs obtained by counting exactly the known vibrational modes of the sample are compared to their semiclassically approximated forms. As a result, the temperature obtained directly from the VDOS differs significantly from

TABLE II. Total emissivity $\varepsilon_{\text{tot}}(s)$ averaged over C_{60} and C_{42} cage carbon cluster families at different temperatures, as obtained from our numerical samples.

	$\varepsilon_{\text{tot}} \times 10^4$	
T (K)	C_{60}	C_{42}
3400	10.6	
2400	7.2	5.9
1350	3.0	2.4

the linear prediction of the semiclassical approximation at low internal energies, as expected and as illustrated in Fig. 9. Because of this additional temperature dependence not accounted for by our simplified model, the total emissivities should be corrected, and we provide in Table II the numerical values of ε_{tot} predicted by our simulations for the cage samples of C_{42} and C_{60}. The values reported in this table show that, even though the analytical model leading to Eq. (22) neglects some size dependence due to the approximate nature of semiclassical densities of states at low energies, it still provides correct orders of magnitude for the emissivity parameter.

V. DISCUSSION

This work suggests that the carriers of thermal emission from hot fullerenes excited by C_{60} desorption [4], collisions with electrons [5], or photoabsorption [7] could be a large set of carbon clusters structurally deviating from ideal fullerenes but having an overall emissivity that scales quadratically with frequency ν. These results have been obtained by considering carbon clusters as isolated systems, allowing us to model radiative emission via recurrent fluorescence in the microcanonical framework. As underlined by previous studies [23,25], a blackbody-like emission requires carriers with continuum absorption spectrum, i.e., without absorption bands. For the present samples of C_{42} and C_{60} carbon clusters, the continuum absorption spectra stem from the equally continuous electronic density of states ρ_{elec} over the sample obtained from accumulating individual, well-resolved electronic absorption spectra at $T = 0$ but assuming no interaction between electronic states or with the vibrational modes.

Our derivation considered only transitions $n \to 0$ back to the ground electronic state; however, intermediate state transitions $n \to m$ are also possible. Assuming that all transition dipole moments associated with these intermediate transitions are constant, it can be shown that these additional transitions favor the emission of high-energy photons (blueshift) and increase the emissivity by about one order of magnitude, as a result of the electronic density of states increasing with energy (see Appendix D). However, this approximation turns out to be rather strong and cannot be verified with the presently available data. Moreover, it still neglects the further contribution of entire emission cascades, which would necessarily produce lower-energy photons and shift the emission spectra back to the red, requiring further corrections to the emissivity that take into account the cooling of the cluster along the relaxation pathway.

In the classical dielectric model [25], the absorption at low energy has a ν^2 dependence, similar to the emissivity found here for a large set of carbon clusters at leading order in $\beta h\nu$ [see Eq. (26)]. However, in the dielectric model this dependence is accounted for by the tail of the Lorentzian shape absorption band associated with surface π-plasmon resonance of buckminsterfullerene, leading to a T^6 dependence in the total emitted power [25]. Our calculation reveals that, while the absorption spectrum increases as ν^2, the total emitted power of a broad structural sample should increase as T^4 [see Eq. (23)], supporting the suggestion of a modified Stefan-Boltzmann relation used earlier to model radiative cooling in several experiments [4,16,19]. However, our simulations show that this dependence is not valid for temperatures below 1500 K because of the quantum nature of vibrational modes. In this regime, the temperature dependence of the total emitted power should grow faster than T^4.

For the samples of C_{60} and C_{42} cages investigated here, the total emissivity ε_{tot} is of the order of 10^{-4}, which is similar to values reported in several experimental investigations [16,18,64,65]. The total emissivity has no explicit dependence on temperature [see Eq. (20)], except indirectly through the values of the parameters U and $\langle R_g \rangle$, which might affect the samples themselves under thermodynamical equilibrium conditions. As underlined by previous studies [16,19], thermal emission is expected to be caused mainly by electronic deexcitation. The present work also supports this conclusion because the oscillator strengths of vibrational normal modes are usually 2–3 orders of magnitude lower than their electronic counterparts. In particular, if vibrational emission were responsible for the thermal emission spectrum, then ε_{tot} would be around 10^{-6}–10^{-8}, which is in contradiction with experimental results. Furthermore, the collective vibrational emission spectrum of a large set of carbon clusters cannot explain a blackbody-like emission in the visible range [26,53].

The emissivity of small particles is usually considered to have a bilinear dependence on their diameter d and on frequency ν as $\varepsilon(d, \nu) \sim \nu d$ [62]. However, the present results from computational samples and TD-DFTB ingredients indicate a different relation, scaling at leading order as $\varepsilon(d, \nu) \sim \nu^2/d^2$.

The ν^2 dependence found for the emissivity is relevant to be further incorporated in astrophysical dust models of carbon clusters emission induced by starlight photon absorption [66–68]. However, it could be even more appropriate to simulate the emission spectrum resulting from the overall radiative cooling of the clusters, especially considering their close connection to very small grains or large carbonaceous molecules being potentially exposed to transient heating under interstellar medium conditions [69].

Laser-induced incandescence (LII) experiments could be modeled in light of the present work to investigate fullerene and soot formation in flames [32]. The experimental estimation of the emissivity and its temperature and wavelength dependences could confirm (or dispute) the approach employed in the present work. However, given the broad size distribution in LII experiments [70], we believe that only the order of magnitude of size carriers might be inferred from the measurement of the total emissivity ε_{tot}.

VI. CONCLUSION

In this work, it was suggested, based on a statistical model, that blackbody-like emissions detected from a sample of hot C_{60} molecules could be explained by emission from a collective set of structurally diverse carbon clusters originating from the isomerization of hot C_{60} rather than from individual hot buckminsterfullerenes, as generally accepted so far. Individually, carbon clusters emit a highly resolved molecularlike spectrum, but it is the statistical average of these molecular spectra over a sample that gives rise to a blackbody-like emission.

From a quantitative perspective, the emissivity of C_{60} or C_{42} samples was found to depend on temperature and frequency as $(\nu/T)^2$ at leading order, the total emissivity amounting to an order of magnitude of 10^{-4}, with a minor dependence on the details of the sample leading to a weak size and structural dependence. The key assumptions needed to reach this result were the approximately linear dependence of the density of electronic states over each sample (Fig. 5) and the lack of correlation between the transition dipole intensity and the energy of the excited state (Fig. 7). Although they were obtained assuming harmonic densities of vibrational states, we believe the generic conclusions should not be drastically affected by anharmonicities, even though the role of intermediate electronic transitions would be worth investigating further in the future.

The results obtained in this work are of potential relevance in the context of interstellar astrochemistry, especially for dust radiative emission and extinction models [66–68]. Recurrent fluorescence from such small carbonaceous species (large carbon clusters, large polycyclic aromatic hydrocarbonlike species, or very small grains [71]) remains to be taken into account in these models, and such an effort would clearly benefit from extending and applying the present modeling.

Our computational approach has also revealed interesting differences with other, well-established models. In particular, the emissivity obtained here differs from the predictions of classical electromagnetism theory, both for the frequency and size dependences. With the aim of bridging the gap between small carbon clusters and larger carbonaceous particles, it would thus be interesting to consider other samples further, allow for the effects of thermal dissociation and a broader distribution of sizes, and disentangle the effects of system size and the properties of electronic excited states and especially their statistical distributions.

ACKNOWLEDGMENTS

This work was supported by the ANR project PACHYNO (Grant No. ANR-16-CE29-0025). O.L. acknowledges the Centre National pour la Recherche Scientifique for funding. We acknowledge GDR Edifices Moléculaires Isolés et Environnés (CNRS GDR 3533) for financial support.

APPENDIX A: ELECTRONIC DATA FOR C_{60} AND C_{42} CARBON CLUSTERS

The entire set of $n \to 0$ transition dipole moments for C_{60} isomers obtained from TD-DFTB calculations are shown in Fig. 7 for the four samples of structures available for C_{42} and C_{60}. These scatter plots do not exhibit any particular correlation between the binding energy and the set of corresponding excited-state energies, allowing us to treat the quantity $U = \langle f(\nu)/\nu \rangle$ as a sample-specific constant.

APPENDIX B: CONTINUUM EMISSION SPECTRUM FROM INDIVIDUAL ISOMER CONTRIBUTIONS

In our approach, the emission spectrum is computed from the accumulation over large numbers of contributions from individual isomers in a sample. Each isomer itself contributes as a sum of discrete contributions at frequencies essentially matching the electronic excited states available for this isomer. The continuous nature of the accumulated spectrum arises from adding these many discrete contributions, but also by convolution with a Gaussian broadening function. In this Appendix we discuss both aspects, illustrating them on the specific sample of C_{60} cages. Figures 8(a)–8(c) show several emission spectra obtained at 3400 K for the same 1000-isomer sample used to generate Fig. 2, but varying the Gaussian broadening with full widths at half maximum of 2.5, 12.5, and 25 meV. Here the continuous character is well established in all cases, the narrowest broadening only producing some limited noise in the spectrum.

The size of the sample also alters the accumulated emission spectrum. Figures 8(d)–8(f) depict the spectra obtained using limited samples of 100, 50, and 10 isomers of C_{60} cages, respectively, keeping a 12.5 meV broadening in the Gaussian convolution. Based on these results, the continuous character of the spectrum is nearly established once 100 isomers are included.

APPENDIX C: EXACT AND SEMICLASSICAL VIBRATIONAL DENSITIES OF STATES FOR C_{60} AND C_{42} CARBON CLUSTERS

In our simulations, the Beyer-Swinehart algorithm [58] is used to exactly compute the vibrational density of states of all carbon clusters, as a function of internal energy, from the knowledge of individual vibrational frequencies. Averaging the resulting densities of vibrational states over entire samples leads to the curves shown in Fig. 9 for C_{60} pretzels and C_{42} cages, taken as representative examples. For comparison, the semiclassical prediction of Eq. (8) obtained with an average zero-point vibrational energy over the corresponding sample is superimposed on the corresponding graphs. The semiclassical approximation is generally found to be valid above about 15 eV for C_{60} samples and above about 10 eV for C_{42} samples.

Figure 9 also shows the variations of the microcanonical temperatures obtained from the calculated vibrational densities of states, following the definition of Eq. (5), for the two samples considered. Deviations are again best seen at low energies, highlighting the range of validity of the semiclassical approximation.

APPENDIX D: CONTRIBUTION OF INTERMEDIATE ELECTRONIC TRANSITIONS

Our model only includes transitions $n \to 0$ relaxing to the ground electronic state. Transitions $n \to m$ leading to intermediate electronic states are also possible, but their treatment

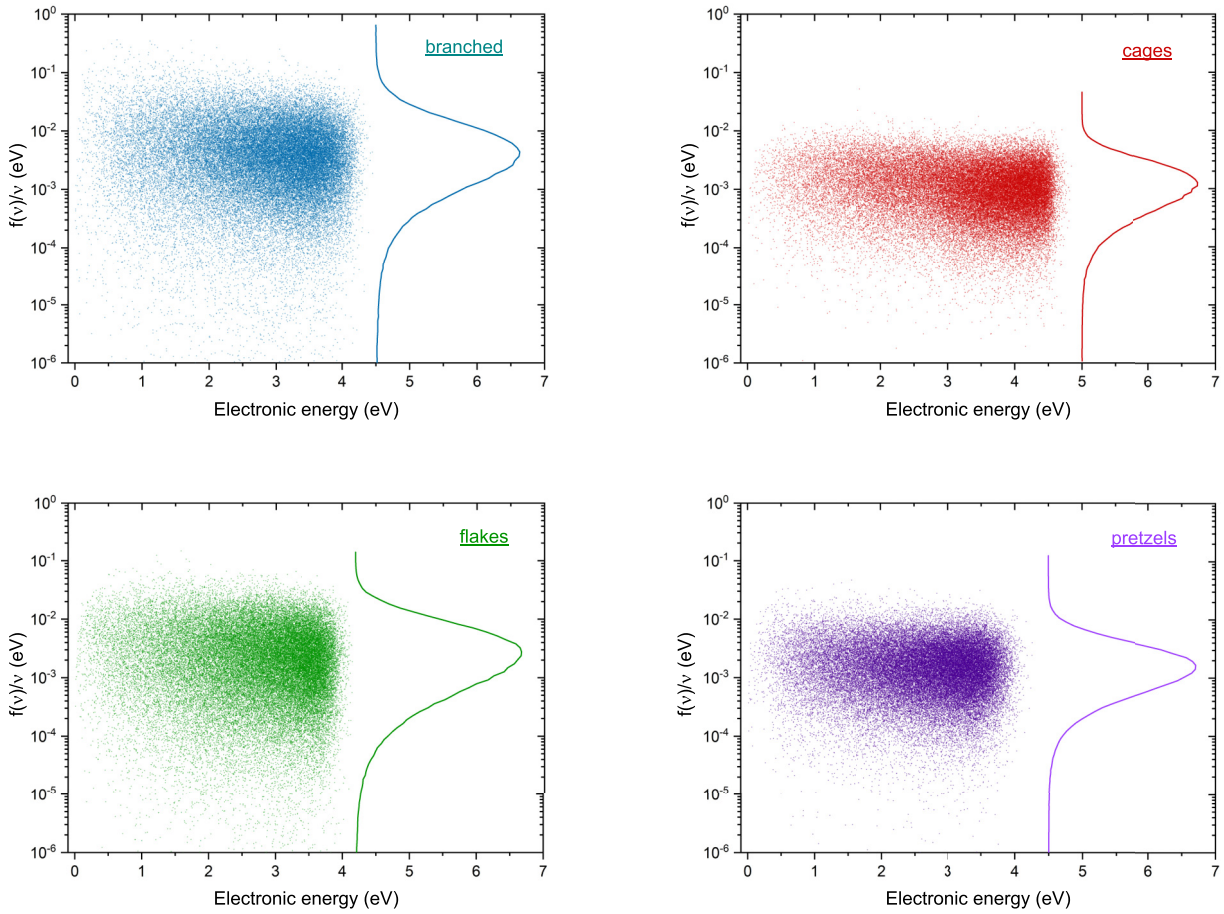

FIG. 7. $n \to 0$ transition moments f_n/ν_n for the $n < 300$ lowest electronic transitions for all isomers of C_{60} considered in this work, sorted in the four determined structural families, each of them containing 1000 isomers, as a function of the corresponding electronic energies. The corresponding densities are also reported.

requires further approximations. We thus assume that the transition dipole moments associated with such transitions are the same as the value for $n \to 0$ transitions averaged over the sample and are given in Table I for each structural family.

Allowing for photons to be emitted from higher-energy states would naturally shift the emission spectrum to the blue and increase the emissivity. To evaluate the new emittance $\overline{M}(\nu, E)$, Eq. (7) can no longer be used because a given photon ν can now originate from various electronic states k, relaxing to states ℓ in such a way that $h\nu = h\nu_k - h\nu_\ell$, where $h\nu_k$ and $h\nu_\ell$ are the energies of these new states. The emittance is thus rewritten as a double sum over all couples of states k and ℓ that precisely can produce such photons,

$$\overline{M}(\nu, E) = \sum_{k>\ell} \frac{h\nu_{k\ell} A_{k\to\ell}}{S} p_k(E)\delta(h\nu - h\nu_{k\ell}), \tag{D1}$$

where we have assumed that the electronic energies ν_k are labeled with k following an increasing order in energy and where $p_k(E)$ is the probability of occupying electronic state k at total internal energy E and $\nu_{k\ell} = \nu_k - \nu_\ell$. Performing a continuous approximation, from the knowledge of the electronic density of states $\rho_{\text{elec}}(h\nu) = Kh\nu$, this probability can be evaluated as

$$p_k(E) \simeq \frac{\beta^2}{K} \exp(-\beta h\nu_k), \tag{D2}$$

in which the semiclassical relation between energy and temperature was again used. Reexpressing the double discrete sum of Eq. (D1) by a double continuous sum and inserting the expression of $p_k(E)$ above and a δ function, we get

$$\overline{M}(\nu, E) \simeq \frac{A(\nu)h\nu}{S}\frac{\beta^2}{K} \times \int_0^E \rho_{\text{elec}}(x)\rho_{\text{elec}}(x + h\nu)e^{-\beta x - \beta h\nu} dx. \tag{D3}$$

The upper limit of the integral can be approximated to infinity, which allows us to solve Eq. (D3) exactly, resulting in

$$\overline{M}(\nu, E) = \frac{A(\nu)}{S}\frac{Kh\nu}{\beta}(2 + \beta h\nu)\exp(-\beta h\nu). \tag{D4}$$

Inserting the original expression of the emittance M_{elec} defined in Eq. (7) in the absence of intermediate transitions, we finally obtain

$$\overline{M}(\nu, E) = M_{\text{elec}}(\nu, E)\frac{K}{\beta^2}\frac{2 + \beta h\nu}{\beta h\nu}. \tag{D5}$$

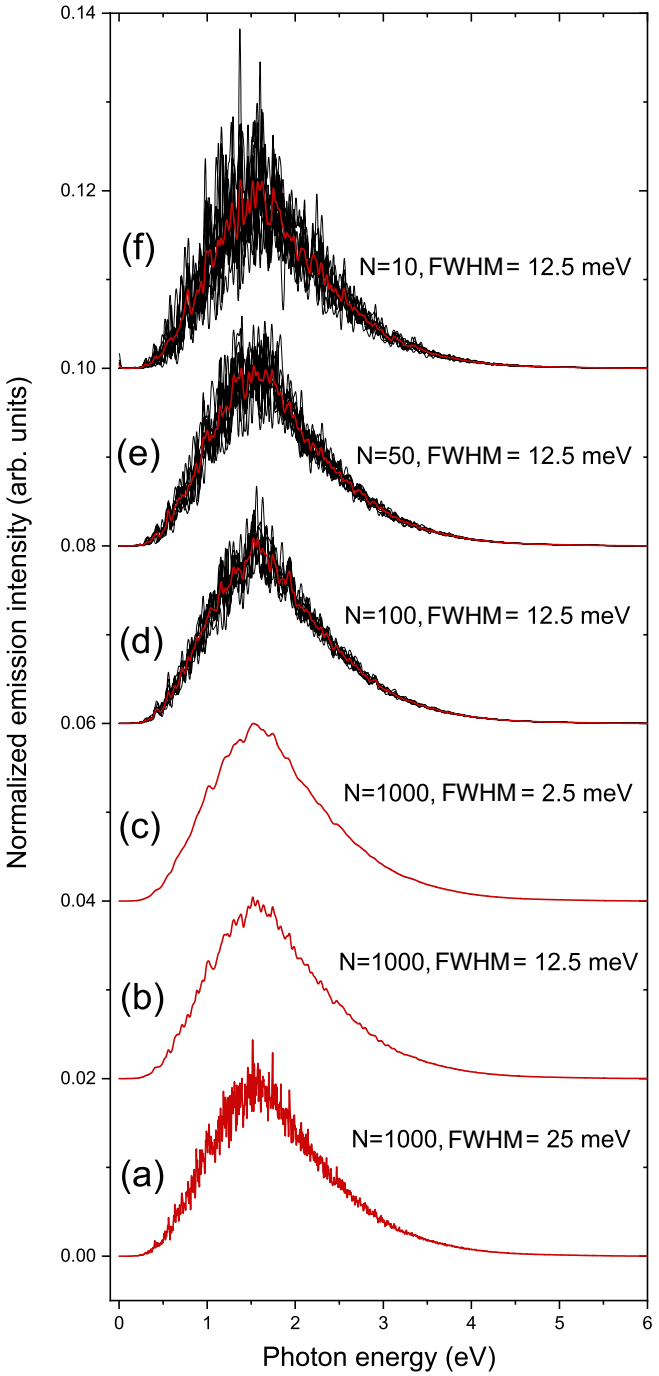

FIG. 8. Emission spectra obtained for C_{60} cages at 3400 K, using different widths for the Gaussian broadening or different sample sizes: (a)–(c) 1000 isomers with widths of (a) 25, (b) 12.5, and (c) 2.5 meV and (d) 100, (e) 50, and (f) 10 isomers but a constant width of 12.5 meV, the result for the 1000-isomer sample being superimposed as a red curve.

Similarly, a total emissivity $\overline{\varepsilon}_{\rm tot}$ can be defined from the integration of $\overline{M}$ over the entire frequency range, at fixed temperature or total energy, as

$$\overline{\varepsilon}_{\rm tot} = \frac{\int_0^\infty \overline{M}(\nu, E)d\nu}{\sigma T^4}, \tag{D6}$$

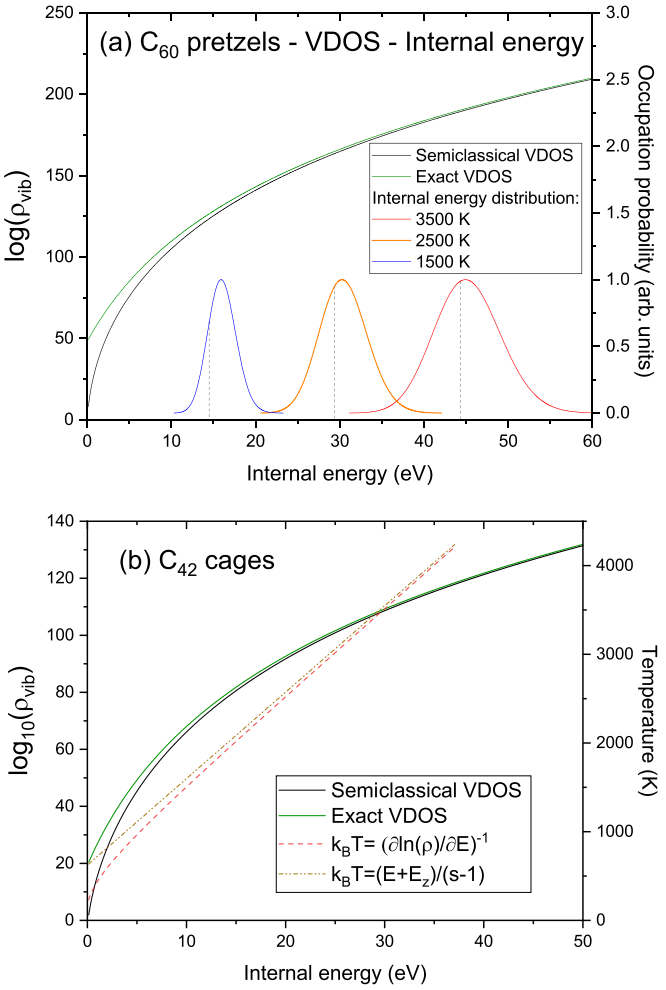

FIG. 9. Vibrational densities of states averaged over the whole sample for (a) C_{60} pretzels and (b) C_{42} cages. The relation between internal energy and temperature is obtained by averaging over the whole sample for (a) C_{60} pretzels. Below 20 eV, the temperatures computed from the exact VDOS and the semiclassical VDOS are significantly different.

which, from Eq. (17), gives the relation

$$\int_0^\infty \overline{M}(\nu, E)d\nu = C(s)K \int_0^\infty \nu^5 \frac{\beta h\nu + 2}{\beta h\nu} e^{-\beta h\nu - (1/2s)(\beta h\nu)^2} d\nu$$
$$= \frac{C(s)}{\beta^4 h^6} \frac{K}{\beta^2} \xi(s), \tag{D7}$$

with

$$\xi(s) = \int_0^\infty x^4 (x+2) \exp\left(-x - \frac{x^2}{2s}\right) dx. \tag{D8}$$

The total emissivity $\overline{\varepsilon}_{\rm tot}$ is then found to be proportional to the value $\varepsilon_{\rm tot}$ obtained for pure $n \to 0$ transitions, with the proportionality factor

$$\frac{\overline{\varepsilon}_{\rm tot}}{\varepsilon_{\rm tot}}(\beta) = \frac{K}{\beta^2} \frac{\xi(s)}{\chi(s)}, \tag{D9}$$

with $\xi(s)$ equal to 151 for C_{60} and 144 for C_{42} and the values of $\chi(s)$ already given in the main text.

For the present systems, the values found for the total emissivity of C_{60} isomers at 3400 K become $10^4 \times \bar{\varepsilon}_{\text{tot}} =$ 9.1, 21.3, 18.9, and 40.1 for the cages, flakes, pretzels, and branched structures, respectively, or approximately one order of magnitude higher than the values reported in Table I.

The above analysis indicates that intermediate transitions could significantly increase the emission rate and total emissivity, but this is a natural consequence of including more emission channels. Furthermore, if intermediate transitions are allowed, then so should be the further possible relaxations to even lower-energy states. Such emission cascades would naturally produce lower-energy photons, but their contribution to the emissivity is less clear because, due to the repeated emission of photons, the temperature should decrease and the reference to the Planck model would become ill-defined.

[1] J. Jortner, Z. Phys. D **24**, 247 (1992).
[2] W. A. De Heer, Rev. Mod. Phys. **65**, 611 (1993).
[3] M. Brack, Rev. Mod. Phys. **65**, 677 (1993).
[4] R. Mitzner and E. E. Campbell, J. Chem. Phys. **103**, 2445 (1995).
[5] A. A. Vostrikov, D. Yu. Yubov, and A. A. Agarkov, JETP Lett. **63**, 963 (1996).
[6] E. A. Rohlfing, J. Chem. Phys. **89**, 6103 (1988).
[7] P. Heszler, J. Carlsson, and P. Demirev, J. Chem. Phys. **107**, 10440 (1997).
[8] G. Walder, K. W. Kennedy, and O. Echt, Z. Phys. D **26**, 288 (1993).
[9] E. Campbell, G. Ulmer, and I. Hertel, Z. Phys. D **24**, 81 (1992).
[10] R. N. Compton, A. A. Tuinman, and J. Huang, in *Proceedings of the Eighth International Symposium on Resonance Ionization Spectroscopy, State College, 1996*, AIP Conf. Proc. No. 388 (American Institute of Physics, Melville, NY, 1997), pp. 21–26.
[11] R. Deng and O. Echt, J. Phys. Chem. A **102**, 2533 (1998).
[12] E. Campbell and R. Levine, Annu. Rev. Phys. Chem. **51**, 65 (2000).
[13] B. Concina, F. Lépine, and C. Bordas, Phys. Rev. A **90**, 033415 (2014).
[14] K. Hansen, R. Richter, M. Alagia, S. Stranges, L. Schio, P. Salén, V. Yatsyna, R. Feifel, and V. Zhaunerchyk, Phys. Rev. Lett. **118**, 103001 (2017).
[15] P. Ferrari, E. Janssens, P. Lievens, and K. Hansen, Int. Rev. Phys. Chem. **38**, 405 (2019).
[16] E. Kolodney, A. Budrevich, and B. Tsipinyuk, Phys. Rev. Lett. **74**, 510 (1995).
[17] K. Hansen and E. Campbell, J. Chem. Phys. **104**, 5012 (1996).
[18] M. Hedén, K. Hansen, F. Jonsson, E. Rönnow, A. Gromov, E. Campbell, A. Taninaka, and H. Shinohara, J. Chem. Phys. **123**, 044310 (2005).
[19] J. U. Andersen, C. Brink, P. Hvelplund, M. O. Larsson, B. Bech Nielsen, and H. Shen, Phys. Rev. Lett. **77**, 3991 (1996).
[20] M. Goto, A. Sundén, H. Shiromaru, J. Matsumoto, H. Tanuma, T. Azuma, and K. Hansen, J. Chem. Phys. **139**, 054306 (2013).
[21] K. Najafian, M. S. Pettersson, B. Dynefors, H. Shiromaru, J. Matsumoto, H. Tanuma, T. Furukawa, T. Azuma, and K. Hansen, J. Chem. Phys. **140**, 104311 (2014).
[22] H. Kataura, N. Irie, N. Kobayashi, Y. Achiba, K. Kikuchi, T. H. T. Hanyu, and S. Y. S. Yamaguchi, Jpn. J. Appl. Phys. **32**, L1667 (1993).
[23] W. Chupka and C. E. Klots, Int. J. Mass Spectrom. Ion Process **167–168**, 595 (1997).
[24] K. Hansen and E. E. B. Campbell, Phys. Rev. E **58**, 5477 (1998).
[25] J. Andersen and E. Bonderup, Eur. Phys. J. D **11**, 413 (2000).
[26] O. Lacinbala, F. Calvo, C. Dubosq, C. Falvo, P. Parneix, M. Rapacioli, A. Simon, and T. Pino, J. Chem. Phys. **156**, 144305 (2022).
[27] M. Hansen, J. Pacheco, and G. Onida, Z. Phys. D **35**, 141 (1995).
[28] S. G. Kim and D. Tománek, Phys. Rev. Lett. **72**, 2418 (1994).
[29] G. von Helden, M.-T. Hsu, P. R. Kemper, and M. T. Bowers, J. Chem. Phys. **95**, 3835 (1991).
[30] G. von Helden, N. G. Gotts, and M. T. Bowers, Nature (London) **363**, 60 (1993).
[31] N. G. Gotts, G. von Helden, and M. T. Bowers, Int. J. Mass Spectrom. Ion Process **149–150**, 217 (1995).
[32] J. W. Martin, M. Salamanca, and M. Kraft, Prog. Energy Combust. Sci. **88**, 100956 (2022).
[33] J. Ahrens, M. Bachmann, T. Baum, J. Griesheimer, R. Kovacs, P. Weilmünster, and K.-H. Homann, Int. J. Mass Spectrom. Ion Process **138**, 133 (1994).
[34] K.-H. Homann, Angew. Chem. Int. Ed. **37**, 2434 (1998).
[35] M. Frenklach and L. B. Ebert, J. Phys. Chem. **92**, 561 (1988).
[36] K. Sellgren, M. W. Werner, J. G. Ingalls, J. Smith, T. Carleton, and C. Joblin, Astrophys. J. Lett. **722**, L54 (2010).
[37] J. Cami, J. Bernard-Salas, E. Peeters, and S. E. Malek, Science **329**, 1180 (2010).
[38] O. Berné, G. Mulas, and C. Joblin, Astron. Astrophys. **550**, L4 (2013).
[39] E. K. Campbell, M. Holz, D. Gerlich, and J. P. Maier, Nature (London) **523**, 322 (2015).
[40] P. W. Dunk, N. K. Kaiser, C. L. Hendrickson, J. P. Quinn, C. P. Ewels, Y. Nakanishi, Y. Sasaki, H. Shinohara, A. G. Marshall, and H. W. Kroto, Nat. Commun. **3**, 855 (2012).
[41] O. Berné and A. G. Tielens, Proc. Natl. Acad. Sci. USA **109**, 401 (2012).
[42] A. Omont and H. Bettinger, Astron. Astrophys. **650**, A193 (2021).
[43] J. Zhang, F. L. Bowles, D. W. Bearden, W. K. Ray, T. Fuhrer, Y. Ye, C. Dixon, K. Harich, R. F. Helm, M. M. Olmstead *et al.*, Nat. Chem. **5**, 880 (2013).
[44] O. Lacinbala, F. Calvo, E. Dartois, C. Falvo, P. Parneix, A. Simon, and T. Pino, Astron. Astrophys. **671**, A89 (2023).
[45] T. Höltzl, P. Ferrari, E. Janssens, and K. Hansen, Phys. Rev. A **106**, 062826 (2022).
[46] A. Léger, P. Boissel, and L. d'Hendecourt, Phys. Rev. Lett. **60**, 921 (1988).
[47] S. Martin, J. Bernard, R. Brédy, B. Concina, C. Joblin, M. Ji, C. Ortega, and L. Chen, Phys. Rev. Lett. **110**, 063003 (2013).
[48] M. Saito, H. Kubota, K. Yamasa, K. Suzuki, T. Majima, and H. Tsuchida, Phys. Rev. A **102**, 012820 (2020).

[49] K. Peeters, E. Janssens, K. Hansen, P. Lievens, and P. Ferrari, Phys. Rev. Res. **3**, 033225 (2021).
[50] Y. Ebara, T. Furukawa, J. Matsumoto, H. Tanuma, T. Azuma, H. Shiromaru, and K. Hansen, Phys. Rev. Lett. **117**, 133004 (2016).
[51] S. Iida, W. Hu, R. Zhang, P. Ferrari, K. Masuhara, H. Tanuma, H. Shiromaru, T. Azuma, and K. Hansen, Mon. Not. R. Astron. Soc. **514**, 844 (2022).
[52] M. A. Bonnin, C. Falvo, F. Calvo, T. Pino, and P. Parneix, Phys. Rev. A **99**, 042504 (2019).
[53] C. Dubosq, C. Falvo, F. Calvo, M. Rapacioli, P. Parneix, T. Pino, and A. Simon, Astron. Astrophys. **625**, L11 (2019).
[54] C. Dubosq, F. Calvo, M. Rapacioli, E. Dartois, T. Pino, C. Falvo, and A. Simon, Astron. Astrophys. **634**, A62 (2020).
[55] M. Elstner, D. Porezag, G. Jungnickel, J. Elsner, M. Haugk, T. Frauenheim, S. Suhai, and G. Seifert, Phys. Rev. B **58**, 7260 (1998).
[56] T. A. Niehaus, S. Suhai, F. Della Sala, P. Lugli, M. Elstner, G. Seifert, and T. Frauenheim, Phys. Rev. B **63**, 085108 (2001).
[57] C. Cohen-Tannoudji, B. Diu, and F. Laloë, *Quantum Mechanics* (Wiley-VCH, Weinheim, 1986), Vol. 2.
[58] T. Beyer and D. Swinehart, Commun. ACM **16**, 379 (1973).
[59] D. W. Brenner, O. A. Shenderova, J. A. Harrison, S. J. Stuart, B. Ni, and S. B. Sinnott, J. Phys.: Condens. Matter **14**, 783 (2002).
[60] C. Lifshitz, Int. J. Mass Spectrom. **198**, 1 (2000).
[61] P. J. Robinson and K. A. Holbrook, *Unimolecular Reactions* (Wiley-Interscience, New York, 1972).
[62] C. F. Bohren and D. R. Huffman, *Absorption and Scattering of Light by Small Particles* (Wiley, New York, 2008).
[63] P. Labastie and R. L. Whetten, Phys. Rev. Lett. **65**, 1567 (1990).
[64] P. Barran, S. Firth, A. Stace, H. Kroto, K. Hansen, and E. Campbell, Int. J. Mass Spectrom. Ion Process **167–168**, 127 (1997).
[65] Y. Nakai, T. Kambara, A. Itoh, H. Tsuchida, and Y. Yamazaki, Phys. Rev. A **64**, 043205 (2001).
[66] M. Compiègne, L. Verstraete, A. Jones, J.-P. Bernard, F. Boulanger, N. Flagey, J. Le Bourlot, D. Paradis, and N. Ysard, Astron. Astrophys. **525**, A103 (2011).
[67] A. Jones, M. Köhler, N. Ysard, M. Bocchio, and L. Verstraete, Astron. Astrophys. **602**, A46 (2017).
[68] B. S. Hensley and B. Draine, Astrophys. J. **906**, 73 (2021).
[69] K. Sellgren, Astrophys. J. **277**, 623 (1984).
[70] H. Bladh, N.-E. Olofsson, T. Mouton, J. Simonsson, X. Mercier, A. Faccinetto, P.-E. Bengtsson, and P. Desgroux, Proc. Combust. Inst. **35**, 1843 (2015).
[71] F. Galliano, M. Galametz, and A. P. Jones, Annu. Rev. Astron. Astrophys. **56**, 673 (2018).